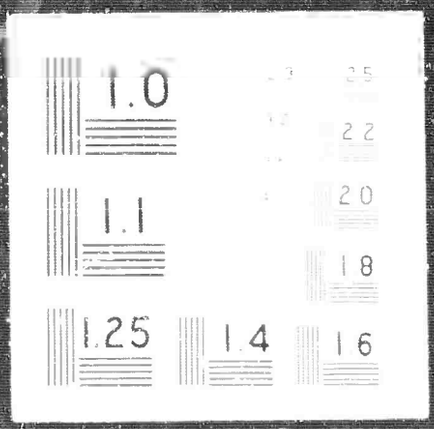

Contract Nonr-4132(00)
Program Code Number 3730
Authorization ARPA Order 306-62
Task Number NR017-710

CZOCHRALSKI RUBY

Semiannual Technical Summary Report

Period: 1 January 1965-30 June 1965

July 29, 1965

M.N. Plooster - Project Scientist
O.H. Nestor - Principal Investigator

This research is a part of Project DEFENDER under the joint sponsorship of the Advanced Research Projects Agency, the Office of Naval Research and the Department of Defense.

Union Carbide Corporation, Linde Division
Speedway Laboratories
P.O. Box 24184
Indianapolis, Indiana 46224

TABLE OF CONTENTS

ABSTRACT

The experimental program on growth of ruby crystals by the Czochralski technique during this report period has emphasized improved control over temperature fluctuations and temperature gradients in the system, to increase still further the homogeneity of the product.

A thorough evaluation of the optical and crystallographic properties of Czochralski ruby is presented, showing the uniformly high quality of the material when grown with preferred orientations. The optical quality of Czochralski ruby ranges from very good for 60° and good for 90° crystals to fairly poor for 0° material. Both 60° and 90° crystals are of exceedingly high crystallographic perfection; 0° crystals are markedly inferior, exhibiting misorientations and dislocation densities of much greater magnitude. The fluorescence linewidth of Czochralski ruby is essentially independent of crystal orientation and is unaffected by annealing; an apparent concentration dependence is observed, with higher linewidths at higher chromium concentration levels.

LIST OF FIGURES

LIST OF TABLES

CZOCHRALSKI RUBY

I. INTRODUCTION

The purpose of the work on Contract No. Nonr-4132(00) is "to develop the technique of growing sapphire uniformly doped with chromic oxide by the Czochralski process." The results of the efforts prior to the present reporting period have been the production of ruby crystals of a size and degree of perfection not previously available by any technique. This report describes the recent efforts to attain growth conditions conducive to production of ruby of a still higher degree of perfection, as is required for the ultimate needs of the ARPA-ONR Laser Program. In addition, a thorough evaluation of the optical and crystallographic quality of the material produced to date is presented, showing the high quality and uniformity of the product of Czochralski ruby growth. Some of the evaluation data was reported in the previous report; it is included in this report again in order that a complete picture of our present state of knowledge of the properties of Czochralski ruby may be presented.

II. RESULTS

A. Growth Techniques:

Continuous improvements in the components and design of the apparatus for Czochralski ruby growth are being made, to enable the optimization of growth conditions and, therefore, of crystal quality. In the current reporting period, changes have been made to bring about (1) improved control of the temperature of the ruby melt; (2) better regulation of thermal gradients in and around the melt and the crystal; and (3) greater control over the shape of the crystal growth interface. Although all three parameters are closely interrelated, they are discussed separately here.

1. Improved Temperature Control:

In past work, two alternative methods for regulating melt temperature have been used, each with certain advantages and drawbacks. In the

first, the thermal input to the system was maintained at the desired level by automatic control equipment, the level being adjusted manually to regulate crystal size and shape. Small, random temperature changes were found to be most effectively minimized by this procedure. However, long-term drift in temperature, due to gradual changes in thermal characteristics of the system or, more predictably, changes in thermal loading caused by the growing crystal itself, required continual trimming of the control settings, a task which is very difficult to perform well by visual observation alone. In the second method, a radiation pyrometer was used to sense the temperature of a spot on the crucible, and the thermal input to the system varied to maintain the temperature of the spot constant. This method effectively eliminated the need to correct manually for long-term drift in thermal characteristics and compensated quite well for the changing thermal load due to the crystal itself. However, uncontrolled changes in thermal input produced occasional deviations from the desired temperature before the control system could react to counteract them.

The two control schemes have been combined in a dual-feedback-loop control system. An inner, fast-response loop controls the thermal input as in the first method above. However, the desired input level is now directly determined by the output of the controller for the second, outer loop, which regulates the crucible temperature as in the second method above. This control system combines the advantages of both earlier methods and largely eliminates their disadvantages. Under ideal conditions, short-term temperature fluctuations will be no more than 0.25 degree C and long-term drift (over several hours) less than one degree, while operating with a ruby melt at about 2100°C. At these levels, the limiting factors in temperature stability are probably no longer to be found in the electronic control apparatus itself; rather, short-term fluctuations due to convective effects in the liquid and long-term drift due to changes in pyrometer sensitivity or in the emissivity of the crucible surface, provide the ultimate limits. We have good evidence that

the major contribution to the remaining rapid fluctuations in crucible temperature are the result of convection currents in the melt.

Recent evidence shows that the absence of rapid temperature fluctuations of the order of one degree C or more in amplitude is a necessary, but not sufficient, condition for the elimination of bubbles and voids in ruby crystals. All high quality crystals grown to date have resulted from runs in which the temperature fluctuations were held near the lower limits described in the preceding paragraph as being ideal growing conditions. The converse statement is not true, however; there are other factors besides temperature fluctuations that affect crystal quality.

2. Control of Temperature Gradients:

The temperature gradients in and surrounding the melt and crystal exert a profound effect upon many of the variables affecting crystal growth. For example: they are the driving force for convection in the melt, which can influence temperature fluctuations, as above; they determine the shape of the isotherms, and thus the growth interface geometry; they influence transport processes occurring in the diffusion layer at the growth interface; and they determine the magnitude of the thermal stresses in the grown crystals.

The much greater optical and crystallographic perfection of Czochralski ruby, as compared with Verneuil ruby, has been attributed in large part to the lower thermal gradients inherent in the Czochralski process as here practiced. In the current reporting period, the temperature gradients have been further decreased by extending the heated zone around the crucible, thus placing it in a nearly isothermal cavity. Convection in the melt was thereby considerably reduced, with the expected increase in temperature stability. A change in the isotherm shapes in the melt was also affected, as evidenced by an increase in the solid angle subtended by the conical growth interface typical of Czochralski ruby. The optical quality of the crystals thus grown, as determined by Twyman-Green interferometry, was not significantly improved by the reduction in thermal gradients, however.

3. Growth Interface Shape Control:

As noted, the growth interface of a typical Czochralski ruby crystal is conical in shape, usually with a small but well-developed facet at the point. A localized variation in chromium concentration along the crystal axis is tentatively attributed to a variation in the effective segregation coefficient in the neighborhood of this point, due either to a singular behavior of the diffusion layer in the liquid in the vicinity of the point or to an orientation dependence of the segregation coefficient which is enhanced by the presence of a well developed facet at the point. If there is a dependence of the segregation coefficient upon orientation, the multiplicity of crystallographic orientations presented by a conical interface might also lead to some variation in chromium concentration over the entire crystal cross section as well. It therefore appeared advantageous to examine the possible methods of generating a planar growth interface, normal to the crystal axis.

The redistribution of heat input to the system as described in section II-A-2 was partially aimed at reducing the radial temperature gradient sufficiently to produce a flat interface. This approach has not yet succeeded entirely. The efficiency of radiant heat transfer in cooling the upper melt surface, plus the fact that the growing crystal itself acts as a substantial heat sink due to its transparency, seem to insure that a radial temperature gradient, decreasing toward the center, will exist. Some reduction in the ratio of radial to axial temperature gradients has been achieved, to be sure, with the resultant increase in included cone angle at the interface noted above.

At high rates of rotation of the growing crystal, on the other hand, essentially flat growth interfaces are observed. This is evidently a hydrodynamic effect, arising from the stirring effect of the crystal upon the melt. Under normal growth conditions, the natural convective flow in the melt is upward along the crucible walls, radially inward toward the center, and downward along the crucible axis, as shown in Figure 1(a). At high rotation rates, however, the crystal acts as a centrifugal pump, drawing liquid up from below

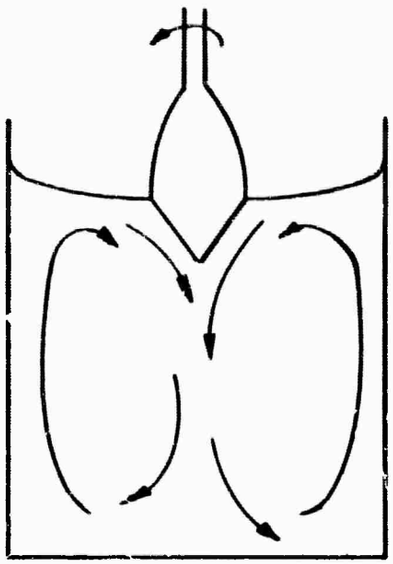

1(a) - LOW CRYSTAL ROTATION RATES · NORMAL CONVECTION

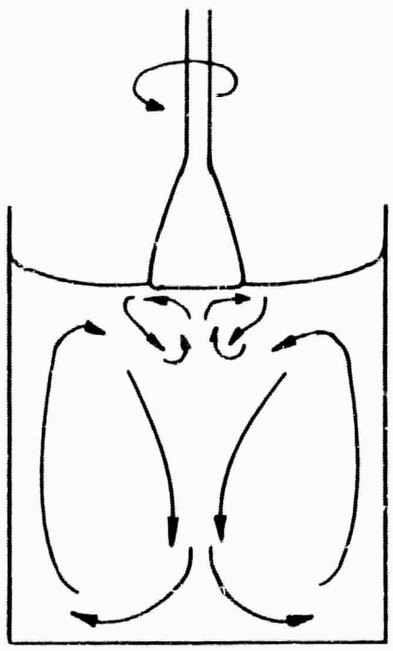

1(b) - HIGH CRYSTAL ROTATION RATES · NOTE "CENTRIFUGAL PUMPING" BY CRYSTAL INTERFACE.

CONVECTIVE FLOW IN RUBY MELT (1a) AND FLOW AS AFFECTED BY HIGH SEED CRYSTAL ROTATION RATES (1b)

FIG. 1

and expelling it radially outward, as in Figure 1(b). The higher linear flow rates past the interface then apparently create a locally flat temperature profile. The increased agitation of the melt unfortunately gives rise to considerable fluctuation in melt temperature and control system instability; crystals grown by this technique to date have been seriously flawed.

B. Optical Quality:

1. Description of Test Procedures:

The optical quality of the crystals is described in terms of the following tests, all carried out on 1/4-inch-diameter laser rods:

a. Schlieren photography, to detect, qualitatively, refractive index variations over the cross section of a rod.

b. Twyman-Green interferometry, to determine variations in optical path length over the cross section of a rod. Adjacent fringes represent optical path variations of one-half wavelength. The 6438A Cd I line is used for this test.

c. Far-field photographs of a collimated beam from a He-Ne gas laser (6328A) after passing through the rod.

d. Far-field energy flux distribution measurements, to determine the angular distribution of the energy flux in the beam described in test (c).

e. High-angle scattering loss measurements, to determine, on a relative basis, the light scattered through large angles by point defects in the rod.

The Schlieren apparatus and the Twyman-Green interferometer are of conventional design and will not be described here. The apparatus for the far-field flux measurment and photographs and for the high-angle scattering measurements are described in the appendices.

2. Results:

The results of the optical measurements can be discussed most significantly in terms of the effects of crystallographic orientation and of the effects of annealing before fabrication upon crystal quality. The Schlieren, Twyman-Green, and far-field photographs for six laser rods, comprising one annealed and one unannealed specimen each of 0°, 60°, and 90° orientation are shown in Figure 2. These rods are all 6.3-mm (1/4-inch) diameter and contain 0.03-0.04 wt % Cr_2O_3. A nominally matching pair of crystals was grown for each orientation, using growth conditions which had previously been optimized for the 60° orientation. (By far the major emphasis in the growth program has been upon the 60° orientation.)

In each figure of this sort in this report, the plane containing the C-axis and the rod axis is in the horizontal direction on the page (except, of course for the case of 0° rods in which case the C-axis is normal to the page.) The rods were examined in light of wavelength and polarization as indicated at the top of each column. (A tungsten filament lamp was used for the Schlieren examinations.) Polarization with the E-vector normal to the C-axis plane is of special interest, since this polarization predominates in ruby lasing.

Working from right to left in Figure 2, the far-field pattern of a gas laser beam after passing through a rod provides an overall appraisal of the optical quality of the rod. In perfect material the pattern would be the system of concentric circular fringes comprising the Fraunhofer diffraction pattern, with 84 percent of the energy in the central (Airy's) disk. That disk covers an included angle of about 0.3 milliradian, or about one-third the dimensioned spacing shown at the right of the figure.

The Twyman-Green interferograms and the Schlieren photographs provide complementary information that indicates the nature of the imperfections causing the departure from ideality in the far-field photographs. The intensity of the shading at any point on a Schlieren photograph is directly related

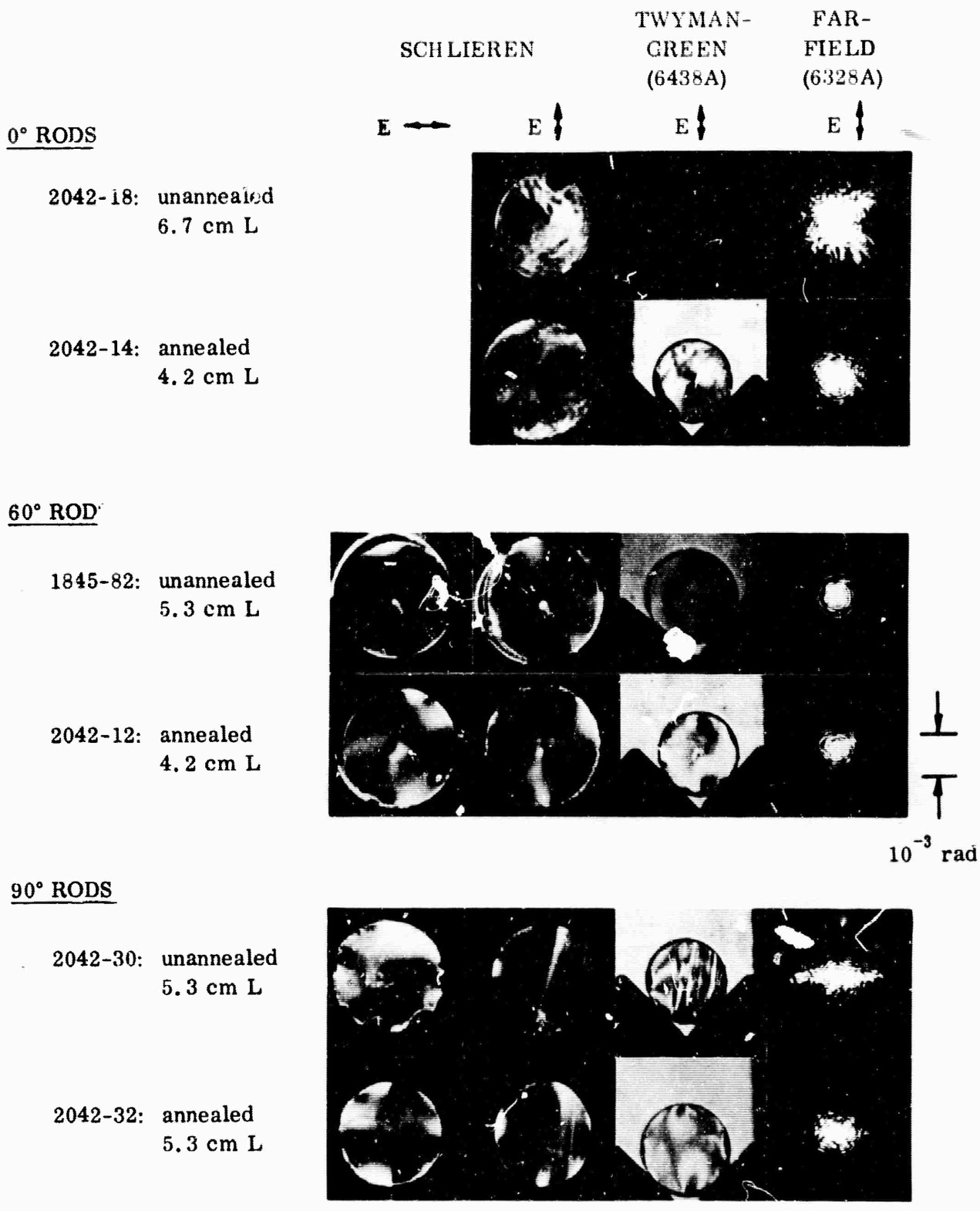

FIG. 2. GROWTH ORIENTATION AND ANNEALING EFFECTS IN CZOCHRALSKI RUBIES (.03-.04 wt % Cr_2O_3). THE C-AXIS PROJECTION ON THE PLANE OF THE PHOTOGRAPH IS HORIZONTAL FOR 60° and 90° RODS. THE PROBE BEAM WAS POLARIZED AS INDICATED AT THE TOP OF EACH COLUMN. THE BEAM WAS LIMITED TO 5.3 mm DIAMETER FOR THE FAR-FIELD PHOTOGRAPHS.

to the gradient in the refractive index across the rod at that point; the interferogram effectively integrates this gradient to give the resultant variation in optical path across the rod.

The 60° Czochralski rubies are seen to be of very high quality. Their far-field patterns approach the diffraction limit quite closely, as will be shown quantitatively later. A practical criterion for diffraction-limited quality, specified by Rayleigh, is that differences in optical paths parallel to the axis of an optical element not exceed $\lambda/4$. In such case, according to Rayleigh, the brightness in Airy's disk would be only 20 percent less than if the element were optically perfect. Others have studied this criterion and generally concur, except that they project a percentage loss from Airy's disk brightness ranging from 11% to 27%. An optical path difference of $\lambda/4$ implies one-half fringe variation in the Twyman-Green photo. This is close to what is found in the interferograms. The Schlieren photographs give no evidence of striae. Both the Schlieren and Twyman-Green photographs disclose the central defect.

Whether considering the far-field patterns, the Twyman-Green interferograms, or the Schlieren photographs, it is evident that quality degrades in the order: 60°, 90°, 0°, annealed or unannealed. Both of the 90° crystals exhibit striations of varying refractive index in planes normal to the C-axis, in the Schlieren photographs and interferograms. The preferential scattering of light in the plane of the C-axis in the far-field photographs is that which would be predicted from the orientation of these striations. No clear explanation for these striations has yet been put forth.

The optical disturbances in the 0° crystals, on the other hand, are randomly oriented, and appear to result from a drastically lower degree of crystallographic perfection than is observed for the 60° and 90° crystals. This subject is pursued in more detail in section II-C of this report.

The far-field energy flux distribution measurements, shown in Figure 3, express quantitatively the information shown qualitatively in the

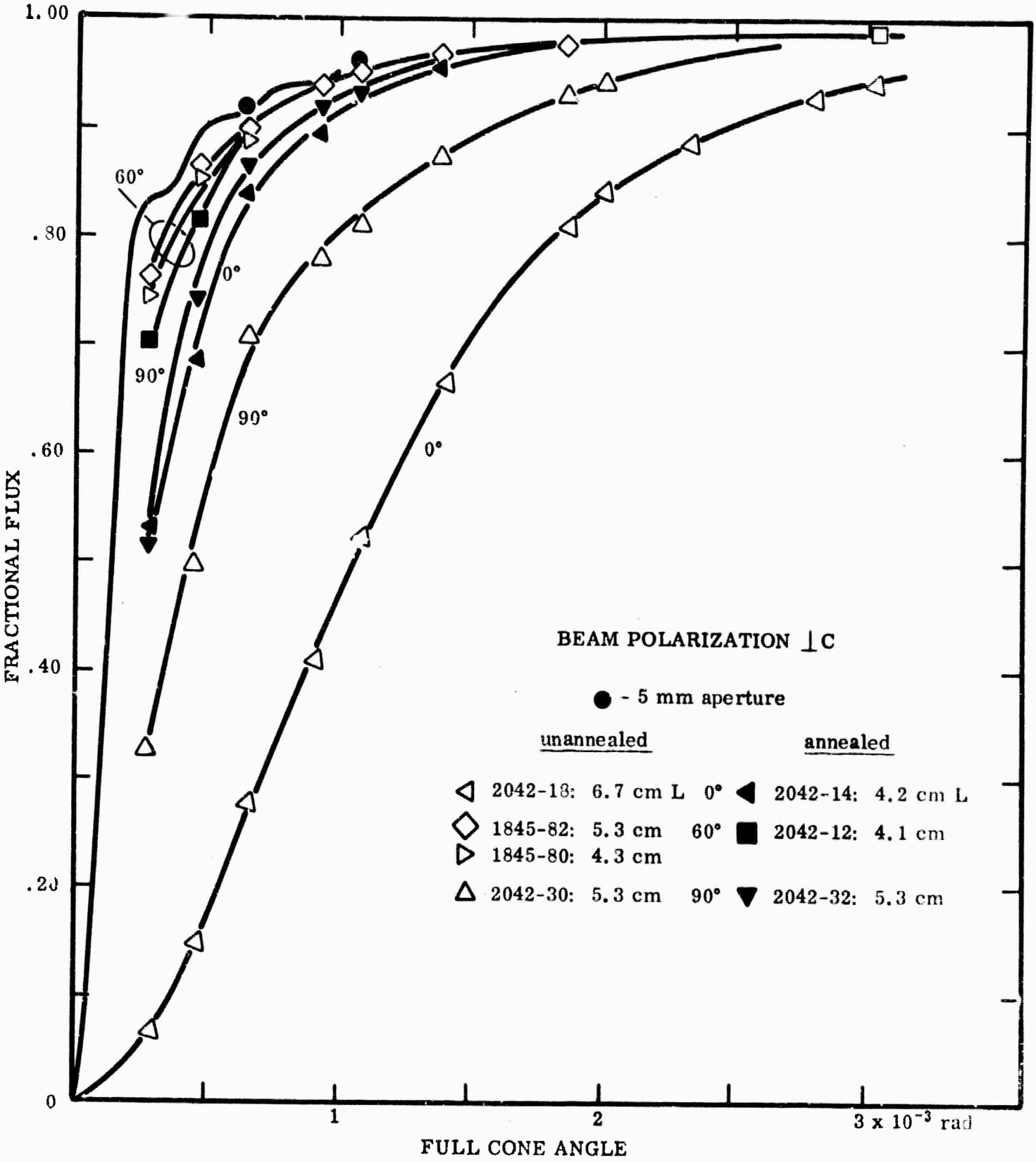

EFFECTS OF GROWTH DIRECTION AND ANNEALING IN CZOCHRALSKI METHOD ON FAR-FIELD FLUX DISTRIBUTION (6328A). THE RODS WERE 1/4 INCH DIAMETER. PROBE BEAM WAS LIMITED TO 5 mm DIAMETER AND WAS POLARIZED NORMAL TO THE C-AXIS.

FIG. 3

far-field photographs. These curves show the fraction of the total energy flux in the beam which is contained within a given beam divergence angle. The uppermost curve on the figure shows the angular energy distribution characteristic of optically perfect material, namely, the Fraunhofer diffraction curve for a 5-mm diameter aperture. It is seen that the 60° ruby rods approach this ideal behavior quite closely. The effect of annealing here is seen to be small; in fact, the annealed rod appears slightly inferior to the unannealed. This is tentatively ascribed to a certain variability in crystal quality from run to run or to variation in the quality of the end finish on the rods, and not to any adverse effect of annealing. In the case of 0° and 90° rods, however, the situation is much different. The annealed rod for each of these orientations is markedly superior to its unannealed counterpart.

The primary sources of optical inhomogeneity in ruby are expected to be refractive index variations due to (a) chromium concentration variation, (b) misorientation, and (c) residual stress. As will be shown, misorientation contributes significantly to the optical properties of 0° ruby, but appears completely negligible in the case of 60° and 90° ruby. The high quality of 60° ruby as grown indicates that here, in addition, residual stresses are very low as well. The marked effect of annealing in 0° and 90° ruby is evidence for the presence of appreciable stresses in these crystals in the as-grown state.

A more conclusive test of annealing would be to examine laser rods fabricated from unannealed crystals, then have them annealed and refabricated, to eliminate the effect of inherent differences between successive crystals. This has not yet been done. However, the variation in quality of Czochralski ruby from run to run is quite low. Figure 4 presents the angular energy flux distribution curves for a number of 60° crystals, both annealed and unannealed, which were grown under a variety of growth conditions (varying growth rates, rotation rates, and atmosphere composition). The consistency in crystal quality, even under varied growth conditions, is immediately evident from this figure. There are two crystals included in this figure which appear remarkably inferior

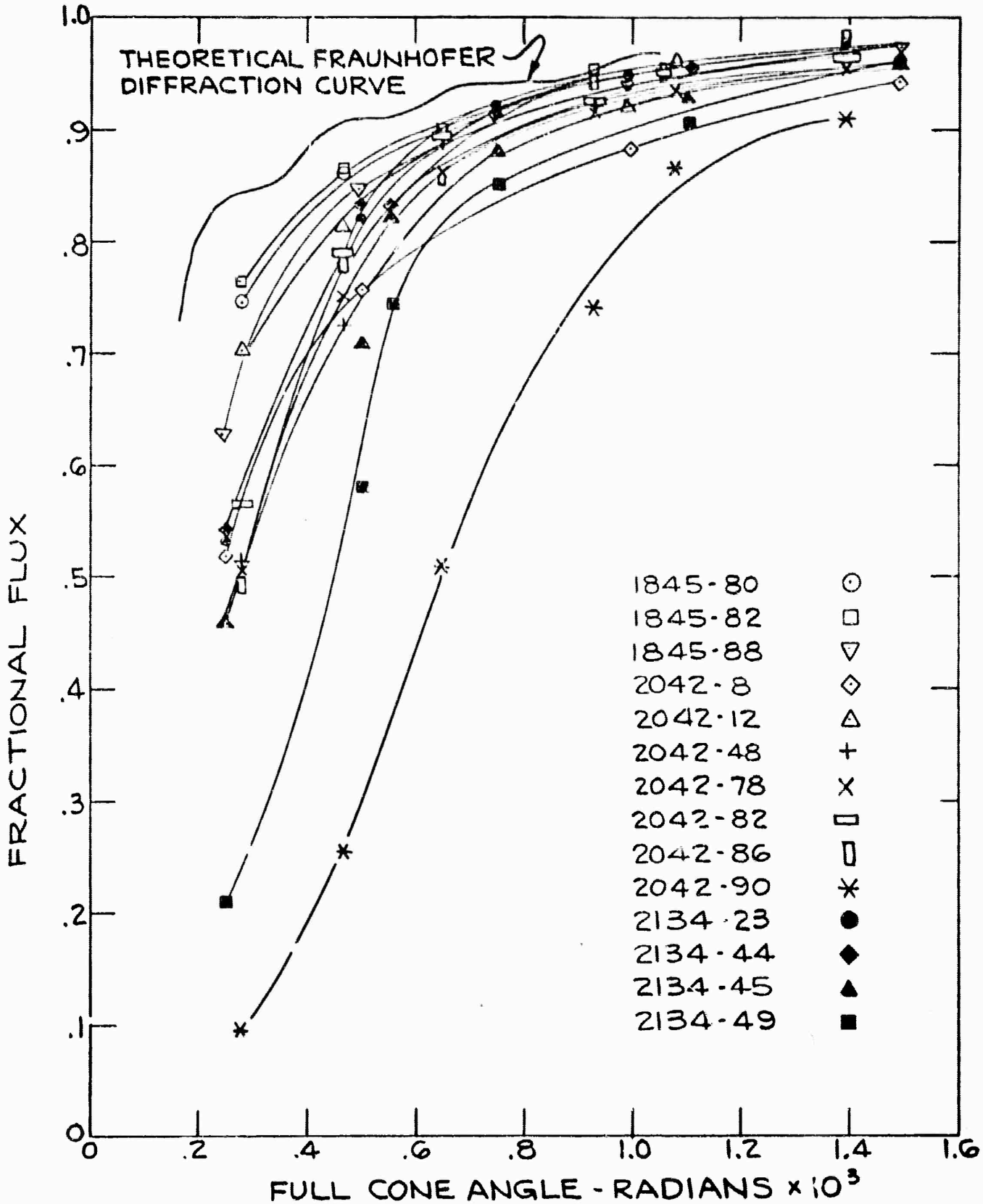

FAR FIELD ENERGY FLUX DISTRIBUTION FOR 14 60° LASER RODS

FIG. 4

to the remainder. In one, 2042-90, the crystal was intentionally doped with about three times the usual amount of Cr_2O_3 and grown at a relatively high pulling rate; the chromium concentration gradients in the crystal were thereby increased by a like amount, and the optical quality suffered accordingly. In the other, 2134-49, longitudinal Schlieren photographs of the crystal disclosed several intense refractive index gradients resulting from changes in the crystal rotation rate during growth. The remainder of the rods show much smaller variation; more importantly, within any group grown under similar conditions, the reproducibility is extremely high.

It has been found that the quality of the end finish on a laser rod can also contribute to its beam divergence curve, especially at small cone angles. Two windows approximately 0.1-inch thick were examined for their effect upon the angular energy flux distribution; since the optical path through these windows was smaller by a factor of 10 to 25 than any of the rods examined, any appreciable dispersion of the beam in passing through these windows is probably due to surface effects. The dispersion curves for these windows are shown in Figure 5, together with the theoretical and experimental values for a simple aperture. From this figure it can be concluded that the quality of the surface finish on the ends of a laser rod can lead to a great apparent variation in the quality of a laser rod, and that the material itself may be considerably better at small divergence angles than is indicated by the flux distribution curves.

The high-angle scattering loss measurements provide a relative measure of the amount of energy lost from a collimated light beam by scattering from point defects in a laser rod. In general, when laser rods fabricated from ruby crystals that contain essentially no visible bubbles, voids, or inclusions are examined by this technique, the measured scattering losses are exceedingly low. The average scattering loss from a number of such rods is about 0.01 percent of the total energy in the incident light beam per centimeter length, and is again quite consistent from one rod to another. This figure is considered so low as to have no significant effect upon the active laser properties of the material.

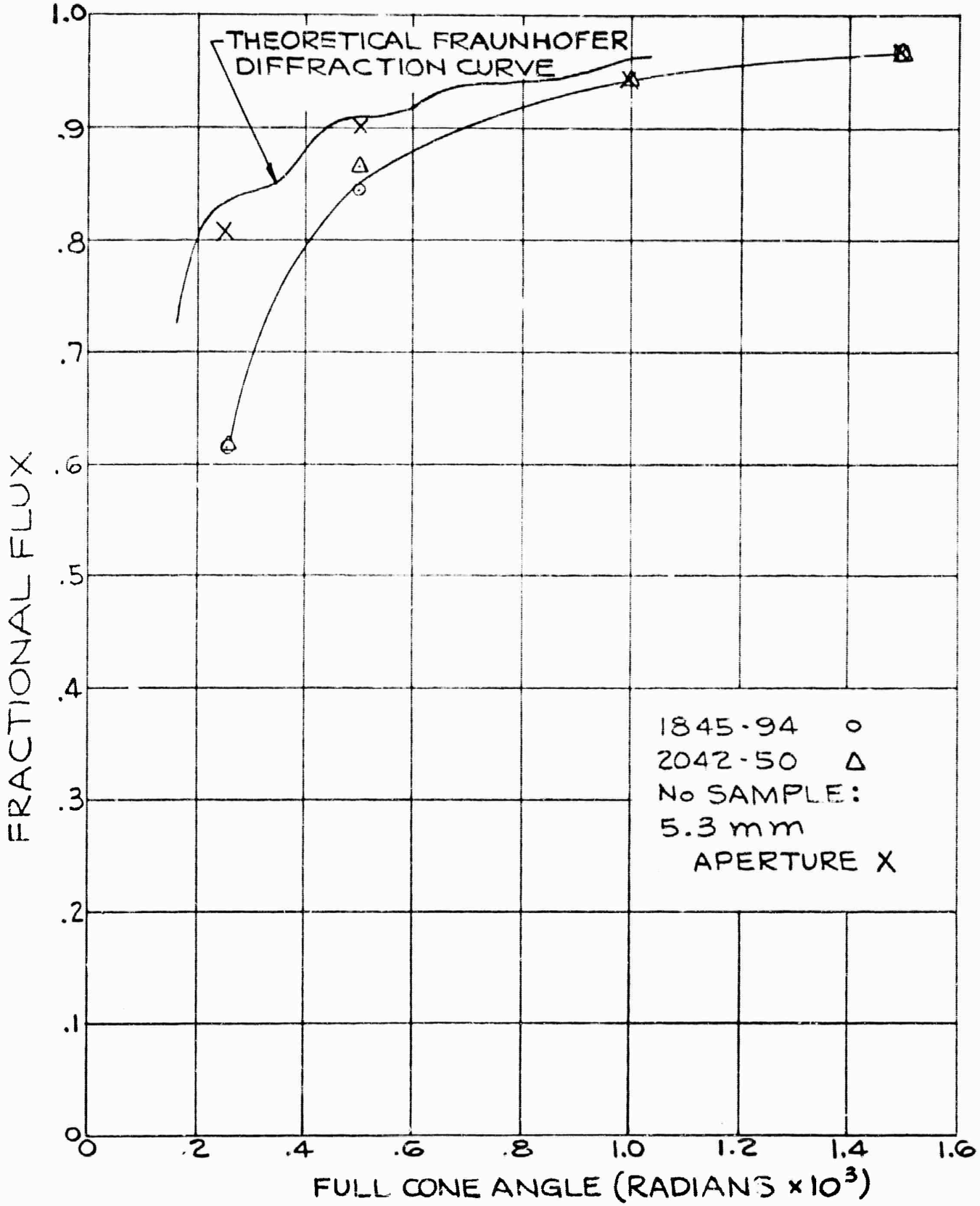

FAR FIELD ENERGY FLUX DISTRIBUTION CURVES FOR TWO 0.1 INCH THICK WINDOWS.

FIG. 5

C. Crystallographic Perfection:

1. Description of Test Procedures:

The following procedures have been used to determine the degree of crystallographic perfection of ruby crystals grown by the Czochralski technique, and are listed roughly in the order of increasing sensitivity:

a. Visual examination under polarized light

b. Examination by Schlieren photography

c. Examination by the Schulz-Wei X-ray diffraction technique

d. Double-crystal X-ray spectrometry

e. Dislocation density determination by chemically etching and counting etch pits

The first two methods rely upon the variation of refractive index with orientation in ruby, and thus are useful only to detect relatively large misorientations, of the order of a degree of arc, within a crystal. The Schulz-Wei technique, as practiced in this laboratory, serves to detect low-angle misorientation boundaries to a lower limit of about two minutes of arc. The double-crystal X-ray investigations were performed by R.D. Deslattes of the National Bureau of Standards and by Birks, Hurley and Sweeney of the Naval Research Laboratory. This method not only serves to detect low-angle misorientation boundaries but also the random mosaic-type misorientation caused by the presence of dislocations scattered throughout a crystal; the method is sensitive down to a very few arc-seconds. And finally, the etch-pit technique allows observation of the individual, elementary deviations from the ideal crystal lattice. The Schlieren and crossed-polar systems require no further description. The Schulz-Wei technique is described in the literature, as is the double-crystal X-ray technique. The etching procedure used for dislocation density measurements here has been described in a previous report.[1]

2. Results:

All examinations of 60° and 90° crystals by polarized light, Schlieren photography, and Schulz-Wei X-ray diffraction have shown no detectable misorientation boundaries within the limits of these methods. With 0° crystals,

however, the results are otherwise, misoriented regions can be seen by all methods. A closer examination of the defects in 0° ruby is profitable for the information it gives concerning the mode of growth and the propagation of defects in Czochralski ruby in general.

The optical quality tests have already shown that a light beam passing through a 0° rod is scattered through relatively large angles and in apparently random directions. The Twyman-Green interferograms, in particular, showed a very irregular, random distribution of imperfections. Visual examination between crossed polars and Schulz-Wei X-ray photographs have shown the presence of many misoriented regions in a typical 0° crystal. A portion of such a Schulz-Wei photograph is shown at the top of Figure 6. Each of the large elliptical spots in the figure corresponds to a single X-ray diffraction spot from the entire surface of the specimen. A point source of X-rays is employed in this method, with the result that a misorientation of one region of the surface of the specimen with respect to another produces a "fracturing" of the spot along the misorientation boundary. In the figure, each spot is seen to consist of a central region surrounded by a large number of wedge-shaped regions, each of which is misoriented with respect to its neighbors.

This singular behavior of 0° ruby suggests that crystallographic imperfections propagate preferentially along the C-axis during growth. Schlieren photographs and dislocation density measurements confirm this hypothesis. At the lower left in Figure 6 a Schlieren photograph of a longitudinal window cut from a 0° boule is shown. Most striking in this photograph is the presence of several longitudinal defects which extend in geometrically straight lines along the entire length of the crystal. (These also stand out under polarized light.) These are almost certainly the misorientation boundaries seen in cross section on the Schulz-Wei photograph. The photograph at the lower right in Figure 6 is of an etched window from a 0° boule, showing the high density of etch pits along the misorientation boundaries and in the many misoriented regions around the periphery of the crystal. Dislocation density measurements in 60° crystals near

FIG. 6

OPTICAL AND CRYSTALLOGRAPHIC DEFECTS IN 0° RUBY CRYSTALS

Schulz-Wei X-ray photograph of 0° crystal

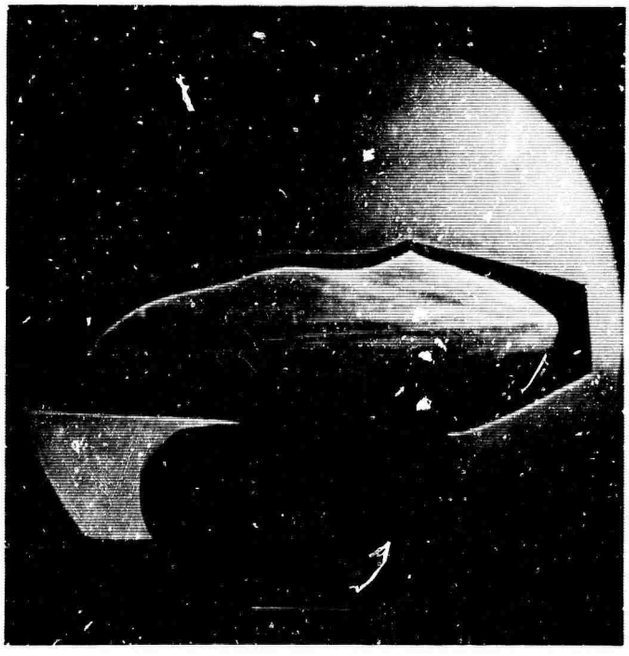

Schlieren photograph of longitudinal section of 0° crystal

Photograph of dislocation etch pits on basal plane of 0° crystal

the seed ends of the crystals have also shown comparable high etch pit densities. In 60° crystals, however, the dislocations soon propagate out to the surface of the crystal and disappear, and material grown subsequently is of much higher perfection.

Dr. R.D. Deslattes of the National Bureau of Standards has kindly examined a one-centimeter cube of Czochralski ruby cut from a 90° boule using a double-crystal X-ray spectrometer.[2] He observed a composite rocking curve at CuKα of about 16 arc-seconds full-width at half-maximum with respect to a first, or reference, crystal of dislocation-free silicon. The reflections operative were the (333) from silicon and the (000-12) from the ruby second crystal. The composite width included dispersive mismatch incurred by using different crystal compositions. Making rough allowance for this, the estimated combined effect of a cold-worked surface and subgrain boundaries was 8 arc-seconds.

Birks, Hurley and Sweeney of the Naval Research Laboratory have made similar measurements on the same crystal after etching the surface.[3] In a paper that has been submitted for publication they report 5 arc-seconds misorientation over millimeter-size areas and 10 arc-seconds over centimeter-size areas.

These figures are rather remarkable. Rayleigh's criterion for diffraction-limited material, when applied to 8-inch-long rubies, translates into a misorientation tolerance of 1/2 degree for 0° and 90° rubies and of 24 arc-seconds for 60° rubies. These are now seen to be satisfied in the 60° and 90° Czochralski crystals.

Double-crystal X-ray measurements have not been made on 60° rods. On the basis of results cited in the foregoing discussion, it is expected that this orientation will be comparable.

Figure 7 shows prismatic edge dislocations (seen in the basal plane) in unannealed 0°, 60°, and 90° Czochralski rubies. A high-density and a

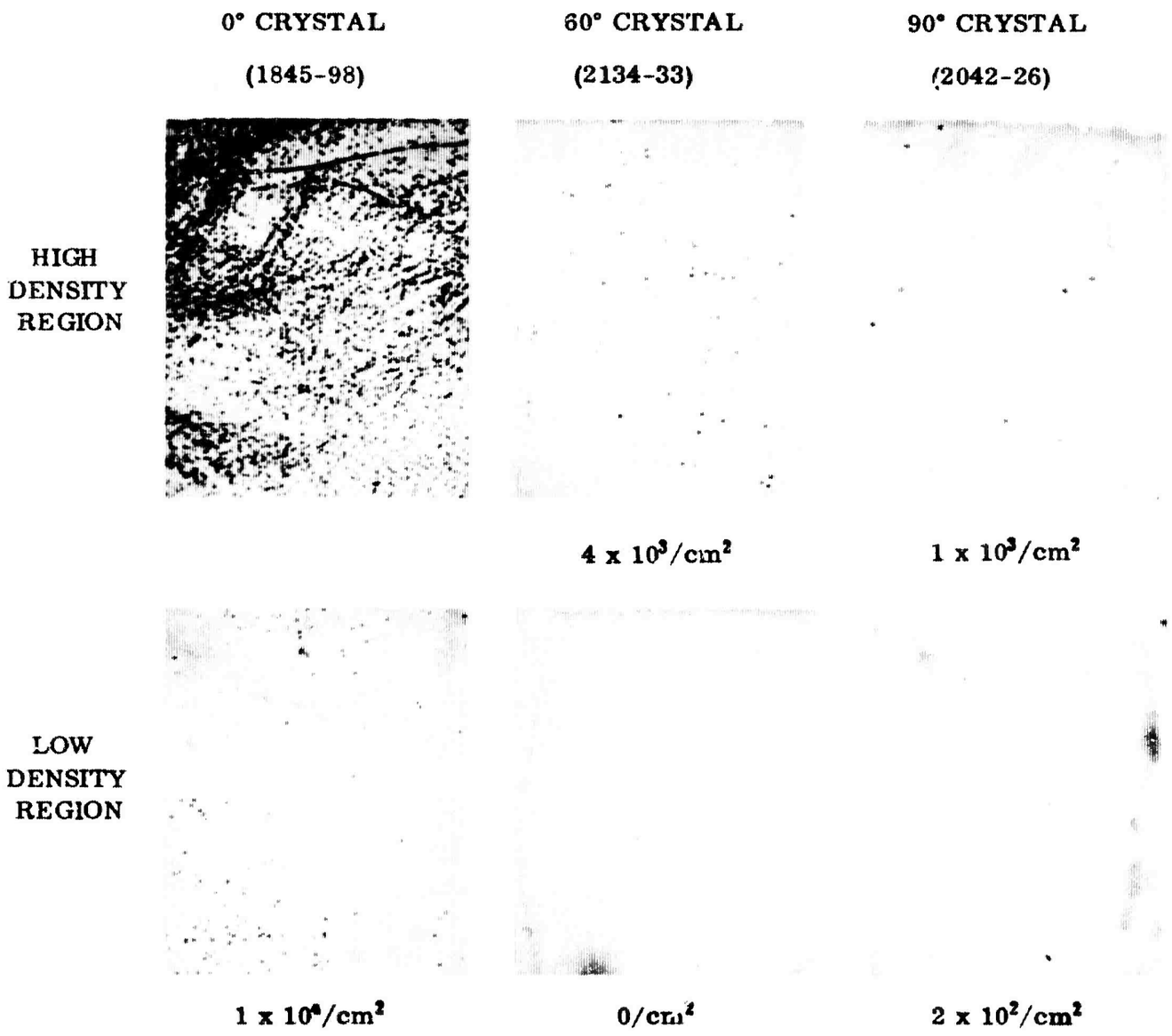

FIG. 7. BASAL-PLANE DISLOCATIONS IN CZOCHRALSKI RUBY. PHOTOGRAPHS REPRESENT 2 mm² AREA.

low-density region was selected for each orientation. Each photograph represents a 2-mm^2 area. The dislocation density determined by etch pit counting is listed below each figure. One etch pit in the 2-mm^2 field gives a density figure of 50/cm^2. The average dislocation density of the 60° and 90° rubies is approximately 1000/cm^2. This is 2-3 orders of magnitude below values reported by Alford and Stephens[4] for Verneuil ruby and sapphire and by Janowski and Conrad[5] for Verneuil ruby laser crystals. There are sizable regions where the density is 100/cm^2 or less, in evidence on the slide, indicating a lower average dislocation density is attainable within the framework of the Czochralski approach. The photographs for the 0° ruby are of selected regions of the sample shown in Figure 6, and illustrate the great difference between 0° material and 60° and 90° material.

D. Fluorescence Linewidths:

The amplification by stimulated emission of a light wave in a laser rod is directly related to the sharpness of the fluorescence line at the laser wavelengths. Fluorescence linewidth measurements on a number of Czochralski ruby laser rods were carried out at liquid nitrogen temperature using a Jarrell-Ash 1.0-meter Fastie-Ebert grating spectrometer with a 7620 lines/inch grating operated in the eighth order. The crystals were placed immediately in front of the entrance slit on the spectrometer and illuminated on the side facing the slit by a mercury arc lamp. Figure 8 shows the arrangement of the optical system for these tests.

The exact determination of fluorescent linewidth is difficult for ruby. The R_1 line is a doublet, with two component lines of approximately equal intensity spaced 0.38 cm^{-1} apart. The individual components are reported to be approximately Lorentzian in shape $\left(I = I_o \left[1 + a^2 (\nu - \nu_o)^2\right]^{-1}\right)$, a fact which was verified by numerically fitting the sum of two Lorentzian curves to a typical spectrometer output trace. At liquid nitrogen temperatures, however, self-absorption effects can be appreciable, resulting in a lowering of the peak intensities and an apparent

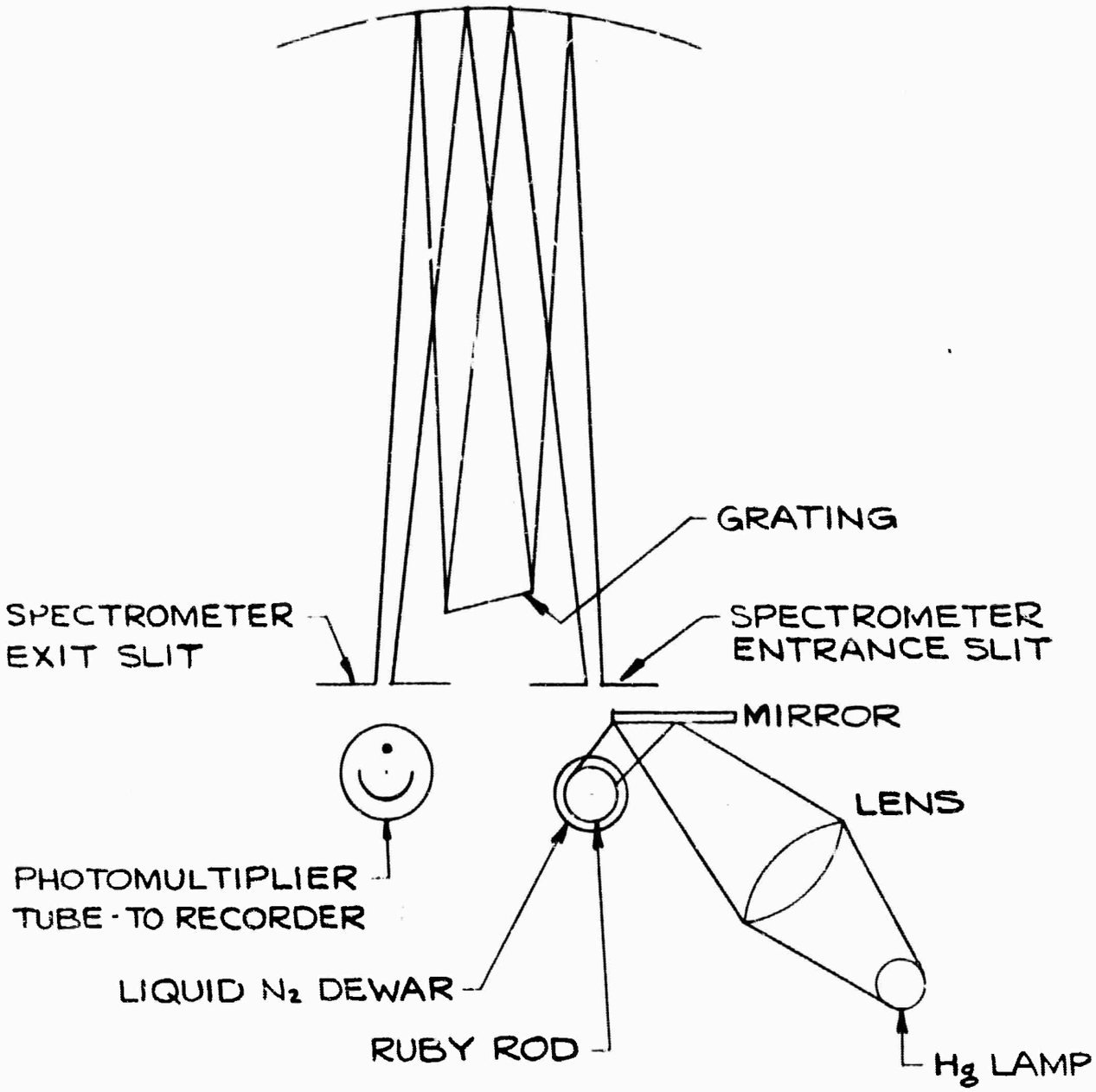

EXPERIMENTAL SET-UP FOR FLUORESCENCE LINEWIDTH MEASUREMENTS.

FIG. 8

broadening of the lines. Measured fluorescence linewidths for 1/4-inch-diameter rods illuminated on the side away from the spectrometer slits were substantially greater than those measured when the rods were illuminated on the side facing the slits. One rod of high Cr content actually exhibited line reversal when illuminated from the back side, with minima appearing in the spectrometer trace where the double maxima appear otherwise. It is probable, therefore, that the values for the linewidths reported here are upper limits and that the true values are lower by some unknown amount. For this reason, a direct comparison with the linewidths reported elsewhere for other ruby crystals is open to question; the data here are intended for internal comparison only.

The linewidths reported here were determined from the ratio of the amplitude of the observed minimum between the two peaks of the fluorescence trace to the amplitude of the peaks themselves. This ratio, for the sum of two Lorentzian curves is given by

$$\frac{I_{min}}{I_{max}} = \frac{4\,\frac{\delta}{\Delta\nu}\left[1+\left(\frac{\delta}{\Delta\nu}\right)^2 - \frac{\delta}{\Delta\nu}\sqrt{1+\left(\frac{\delta}{\Delta\nu}\right)^2}\right]}{\left[1+\left(\frac{\delta}{\Delta\nu}\right)^2\right]^{3/2}}$$

where $\delta = 0.38\ cm^{-1}$ is the separation between the components of the doublet and $\Delta\nu$ is the width of the component lines at half amplitude. The value of this ratio vs. $\Delta\nu$ is plotted in Figure 9.

This method of measurement assumes that I_o and $\Delta\nu$ are the same for both of the component lines of the doublet. In general, from the symmetry of the observed data, these assumptions seem valid. The relative intensities of the two components could be varied somewhat by varying the orientation of the crystal with respect to the spectrometer slit; nearly symmetrical curves were always obtained when the plane containing the C-axis and the rod axis was aligned along the optical path into the spectrometer. In the use of the 0° rods, however, some asymmetry was always present, the long-wavelength component being

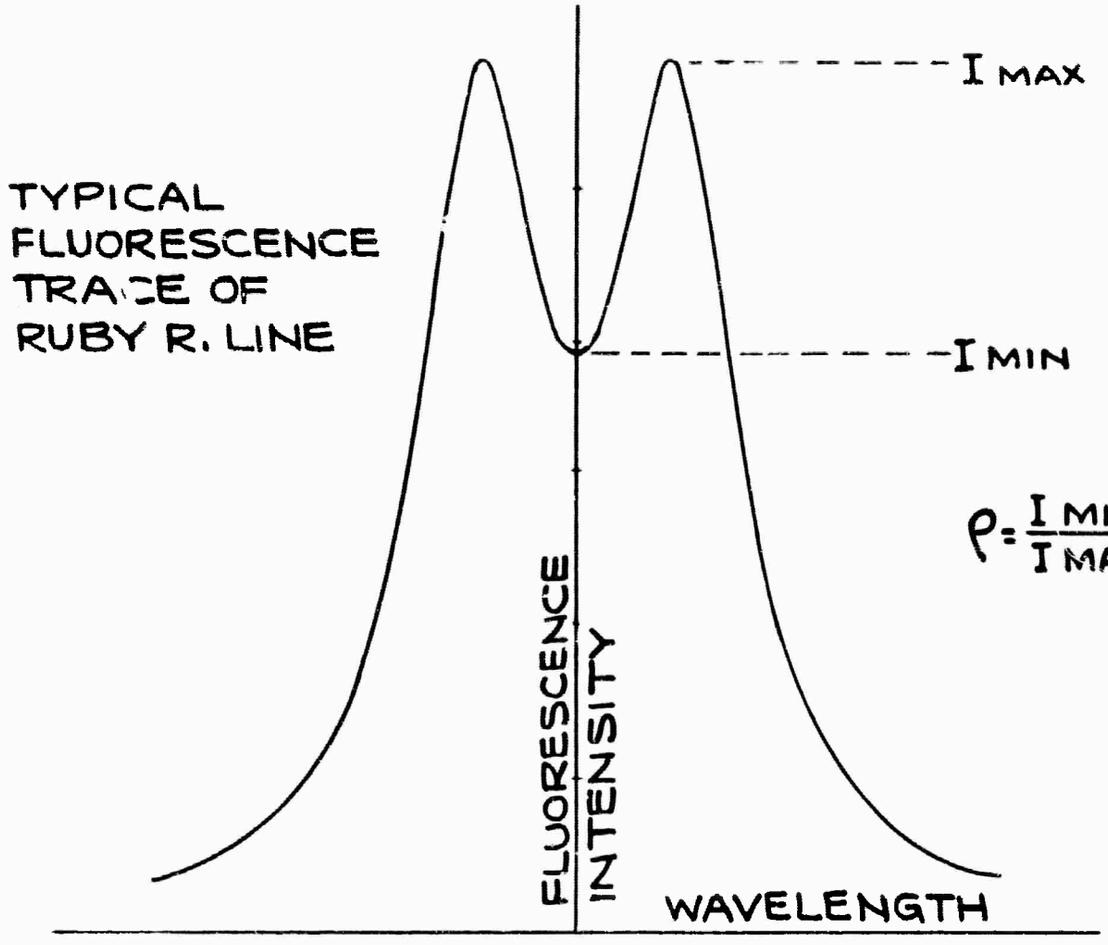
TYPICAL
FLUORESCENCE
TRACE OF
RUBY R. LINE
I MAX
I MIN
$\rho = \frac{I_{MIN}}{I_{MAX}}$
FLUORESCENCE
INTENSITY
WAVELENGTH

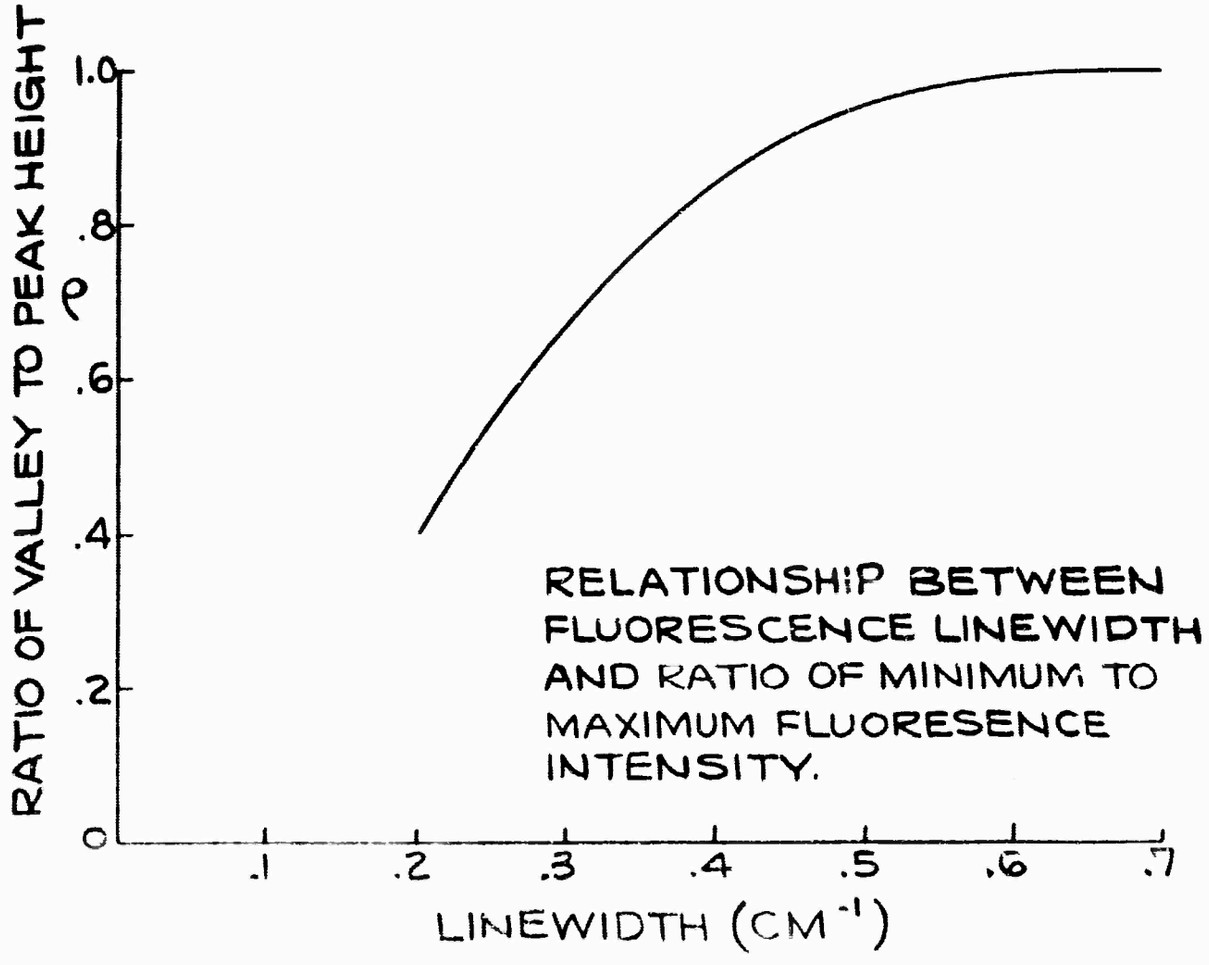
RATIO OF VALLEY TO PEAK HEIGHT
ρ
1.0
.8
.6
.4
.2
0
.1
.2
.3
.4
.5
.6
.7
LINEWIDTH (CM^{-1})
RELATIONSHIP BETWEEN
FLUORESCENCE LINEWIDTH
AND RATIO OF MINIMUM TO
MAXIMUM FLUORESCENCE
INTENSITY.

stronger by about 20 percent. The average of the peak heights was always used in determining the ratio I_{min}/I_{max}; numerical estimates showed that this results in too low a value for the linewidth when the peak heights differ appreciably. Thus the linewidths reported for the 0° ruby in this report are probably somewhat too low in comparison with the values reported for 60° and 90° ruby.

The measured linewidths for 19 Czochralski ruby crystals are given in Table I. The table is divided into annealed and unannealed columns for each growth orientation; furthermore, the crystals are separated within these categories into groups of crystals grown under substantially the same growth conditions. The remarkable fact about the majority of the data is its uniformity. The effect of annealing is seen to be nil; orientation also seems to have but little effect on linewidth. The lowest linewidth is exhibited by a rod of very low chromium concentration; the highest by crystal 2042-90, which was doped with three times the normal Cr content. Part of this apparent concentration dependence is undoubtedly due to broadening of the observed lines by self-absorption. It is also interesting to note that the two crystals exhibiting the highest linewidth are also those which gave the poorest performance in terms of angular dispersion of a light beam (see Figure 4).

E. Active Laser Tests:

Some work has been done on the laser properties of Czochralski ruby; however, it has not been carried to the point that a relatively complete description of its lasing behavior can be presented at this time.

TABLE I. Fluorescence Linewidth Measurements on Czochralski Ruby

Unannealed Crystals		Annealed Crystals		Remarks
Sample Number	Linewidth cm^{-1}	Sample Number	Linewidth cm^{-1}	
0°		0°		
2042-18	.33	2042-14	.32	Slow growth rate
60°		60°		
1845-80	.37			
1845-82	.38	2042-12	.35	Slow growth rate
1845-88	.34	2042- 8	.35	Fast growth rate
2042-48	.36	2042-78	.36	Fast growth rate--
2042-82	.33	2042-86	.35	different atmosphere
2042-90	.44			Cr_2O_3 content 0.1%
2134-23	.34			Different growth
2134-44	.33			apparatus--new
2134-45	.35			temperature control
2134-49	.42			system
90°		90°		
2042-30	.37	2042-32	.37	Slow growth rate
1529-79	.21			Cr_2O_3 content 10 ppm

All crystals 0.03-0.05 wt % Cr_2O_3 unless otherwise noted.

III. FOLLOW-ON PROGRAM

The optical quality of our Czochralski ruby has steadily improved during the last year. In passive beam divergence tests of some recent crystals, the energy included within the Airy's disk was 74%, compared to the diffraction limit of 84%. The crystal quality as measured by passive tests of the best material grown therefore is very close to the ultimate requiremerts set by ONR at the beginning of the contract. Further improvements are still likely, particularly by the further reduction of remaining strain. Continuation of annealing studies is therefore planned. A group of crystals will be fabricated, subjected to several annealing cycles, refabricated and optical quality determined in an effort to select an optimum annealing procedure. Several approaches to further reduce the radial chromium variation will be evaluated.

However, at this stage, greatest contribution to further enhancement of ruby as a laser can be gained from the study of lasing behavior of the best quality Czochralski ruby. We plan to measure lasing parameters such as active beam divergence, active far-field pattern and power output under controlled conditions and correlate these to the previously determined passive tests.

Damage during lasing is also a very significant factor which determines the usefulness of a material. Rods will be intentionally damaged, conditions leading to damage determined and causes for damage sought.

REFERENCES

1. "Czochralski Ruby," Union Carbide Corporation, Linde Division Speedway Laboratories, July 8, 1964

2. R. D. Deslattes--private communication

3. Birks, Hurley and Sweeney--to be published

4. D. L. Stephens and W. J. Alford, J. Am. Ceram. Soc. 47, 81 (1964)

5. K. R. Janowski and H. Conrad, Trans. of Metallurgical Soc. of AIME 230, 717 (1964)

APPENDIX I

BEAM DIVERGENCE MEASUREMENT

Beam divergence measurements reported herein comprised probing the far-field pattern of the light beam with a circular aperture of variable diameter centered on the beam axis and measuring photoelectrically the flux passing the aperture. The flux value was expressed as the fraction of that measured with full aperture and is reported as a function of the full cone angle in the far field.

A schematic of the optical system is shown in Figure 10. The gas laser was a Spectral Physics Model 115 He-Ne laser operating at 6328A. The beam was expanded approximately 14X and was then measured to be of uniform intensity to within 8 percent over a 1.6-cm-diameter aperture in the plane of incidence on the test specimen. The pair of lenses following the test specimen formed and magnified the far-field image of the transmitted beam. In the image plane of this system, where the variable iris was located, the far-field cone angle selected by the aperture typically amounted to 0.1-0.2 milliradian per millimeter diameter opening in the present system, depending on the lens combination used. The lens following the iris collected the transmitted flux into an integrating sphere whereby photodetection could be utilized while maintaining uniform illumination of the photocathode.

The iris-collector lens combination provided an effective aperture range of 2.5-35. mm diameter, equivalent to a cone angle range of 0.25-3.5 milliradians in the higher magnification arrangement of the present system and 0.5-7 milliradians in the lower magnification. The F = 1 fraction flux value reported herein was that obtained for a cone angle of 7 milliradians.

Test rods were positioned in the apparatus so that the C-axis projection in the plane normal to the beam was normal to the polarization direction of the beam. The rod face toward the gas laser was set normal to the beam. The axis of the

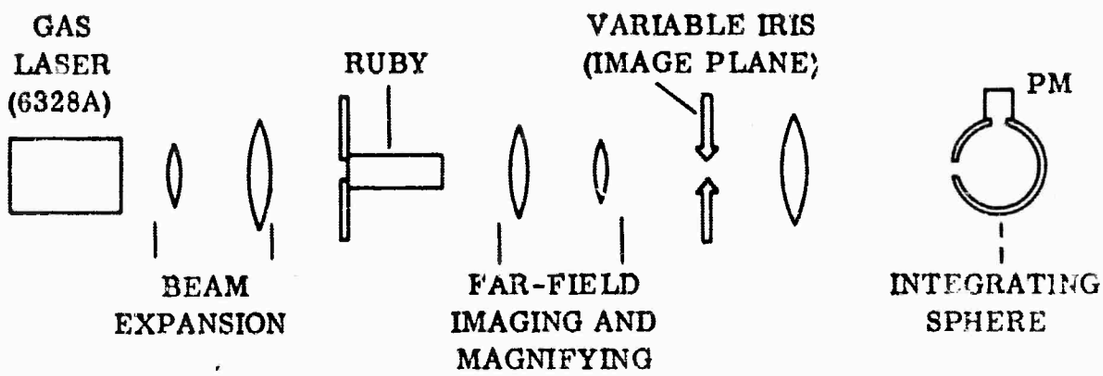

APPARATUS FOR MEASURING THE FAR-FIELD ENERGY FLUX DISTRIBUTION

FIG. 10

transmitted beam was then displaced from the optic axis of the system by the measure of effective optical wedge of the test specimen. In any event the measurements were made with the variable aperture centered on the region of maximum intensity in the far-field pattern.

APPENDIX II

HIGH-ANGLE SCATTERING MEASUREMENT

The high-angle scattering results reported herein refer to the light scattered through the lateral surface when a beam traverses a cylindrical rod axially.

The apparatus, designed to take 1/4-inch-diameter rods, is illustrated in Figure 11. The light source was a tungsten lamp. The radiation from this was collimated, apertured to 4-mm diameter, and filtered to develop a beam of 100 Angstrom bandwidth centered at 7800 Angstroms so as to avoid fluorescence of the ruby R-lines. The probe beam passed through two co-linear tubes that held the test specimen within an integrating sphere while exposing a 1-cm length of the specimen (with ground cylindrical surface) at the center of the sphere. The specimen was moved along its length in 1-cm increments; at each position the photosignal representing scattered flux was recorded and an average for the full sample was determined. The mean deviation amounted typically to 10 percent of the average. A measure of the flux incident on the rod was obtained by replacing the test specimen with a glass rod with polished, inclined end face located centrally in the sphere and oriented to avoid direct reflection onto the photocathode surface. The ratio of the average signal from the specimen to that due to the incident flux, corrected for non-linear system response, is reported herein as the high-angle scattering index.

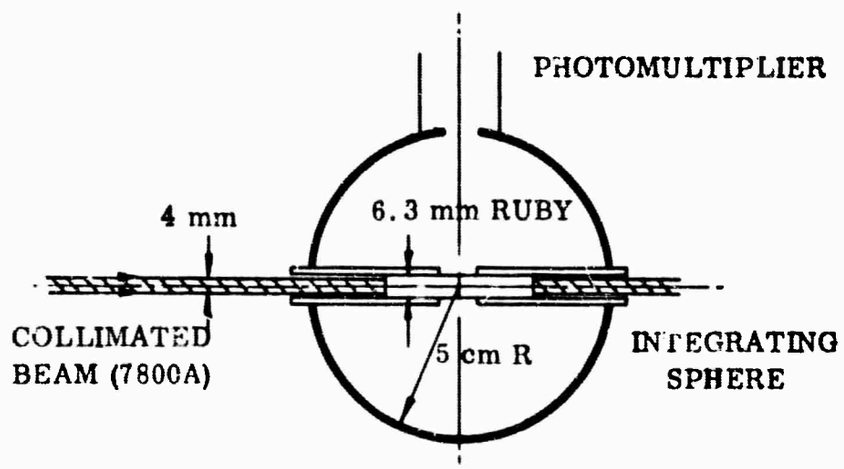

HIGH-ANGLE-SCATTERING MEASUREMENT SCHEME

FIG. 11